Anisotropic Optical Properties of Thin-Film Thiacarbocyanine Dye Aggregates

ARTICLE *in* THE JOURNAL OF PHYSICAL CHEMISTRY C · OCTOBER 2013

Impact Factor: 4.77 · DOI: 10.1021/jp407056t

THE JOURNAL OF PHYSICAL CHEMISTRY C

Article

pubs.acs.org/JPCC

Anisotropic Optical Properties of Thin-Film Thiacarbocyanine Dye Aggregates

K. Roodenko,*[,†] H. M. Nguyen,[‡] L. Caillard,[†] A. Radja,[‡] P. Thissen,[§] J. M. Gordon,[‡] Yu. N. Gartstein,[‡] A. V. Malko,*[,‡] and Y. J. Chabal[†]

[†]Department of Materials Science and Engineering (MSE) and [‡]Department of Physics, University of Texas at Dallas, Richardson, Texas 75080, United States

[§]Institute of Functional Interfaces (IFG), Karlsruhe Institute of Technology, Hermann-von-Helmholtz-Platz 1, 76344 Eggenstein-Leopoldshafen, Germany

ABSTRACT: Optical properties of thin films of aggregated thiacarbocyanine (TCC) dyes have been studied by means of spectroscopic ellipsometry and polarized IR spectroscopy. The experimental results reveal a strongly anisotropic response of the films, as quantified in the reported anisotropic dielectric functions over a wide range of frequencies. The studied TCC films exhibit both J-aggregate and H-aggregate absorption bands with different polarization properties. A strong dielectric resonance arising from the J-aggregate electronic excitations was found to be polarized along the film. The observations are consistent with the preferential orientation of aggregate filaments along the films. We have also used the measured anisotropic properties in model calculations of energy transfer into thin films of J-aggregates to illustrate the potential importance of accurate optical characterization in engineering aggregate-based hybrid nanostructures for optoelectronic applications.

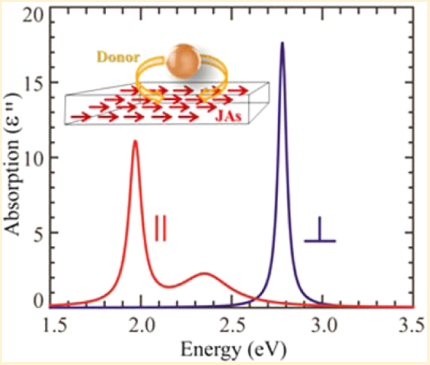

INTRODUCTION

Aggregates of the cyanine dyes are a class of fluorophores with greatly enhanced absorption and emission properties resulting from the coherent coupling of tens to hundreds of planar monomer molecules aligned in a column. Tuning the aggregate structure influences the intermolecular excitonic interactions that couple electric-dipole optical transitions of the individual molecules in the aggregate. When the absorption band of the aggregates is red-shifted (bathochromic shift) in comparison with the monomer absorption band, the aggregates are known as J-aggregates[1] (JAs). Alternatively, aggregates with the blue-shifted (hypsochromic) absorption bands are known as H-aggregates (HAs). The absorption shift depends on the slippage angle between the long axis of an individual molecule and the line-of-centers in a molecular column. Small slippage angles ($\gtrsim 32°$) lead to bathochromic shifts, while large slippage ($\gtrsim 32$) results in a hypsochromic shift.[2,3] Cyanine dyes have been known for many decades and used in photography and in biology.[4] Their aggregation properties in solutions[3,5,6] and in the thin-film form at the liquid−solid interfaces[7] continue to be actively studied. It has also been demonstrated recently that JAs can be utilized in conjunction with tunable and versatile donor fluorophores, such as nanocrystal quantum dots (NQDs). The resulting NQD/JAs hybrid nanostructures could be an attractive materials system for use in optoelectronics applications,[8] for example, in light-emitting diodes[9] and light harvesting assemblies.[10,11]

Despite the growing interest in aggregate-based hybrid structures, optical properties of thin aggregate films remain underexplored. This particularly concerns anisotropy of their optical constants and its dependence on the film preparation. A recent reflectance and transmittance study[7] of thin films of so-called TDBC J-aggregates reported a very substantial peak value $\simeq 10^6$ cm^{-1} of the absorption coefficient. This finding highlights the potential of these materials for applications in optoelectronic devices and calls for more detailed studies of thin-film properties by methods that can detect anisotropy while relaxing the isotropic distribution assumption.[12−14] A good example of such approach is ellipsometric measurements of nonaggregated copper phtalocyanine thin films,[15] which were found to exhibit uniaxial anisotropy. Moreover, it was reported[15] that even the small difference in the molecular tilt angle can lead to pronounced differences in the anisotropic dielectric response. With JAs having an intrinsically anisotropic structure (molecules aligned in the general "head-to-toe" direction), anisotropy of the dielectric response can be expected in thin films as well. Among other things, anisotropy of dielectric properties can affect energy transfer processes as was illustrated recently for the case of transfer into organic crystals.[16]

In this paper, we study anisotropic optical properties of thin films made of the thiacarbocyanine (TCC) aggregated dyes that exhibit both JA and HA absorption bands. TCC dyes[2,3,17] (Figure 1) have attracted attention due to the possibility to tune the absorption line of their molecular aggregates by

Received: July 16, 2013
Revised: September 5, 2013
Published: September 6, 2013

   dx.doi.org/10.1021/jp407056t | J. Phys. Chem. C 2013, 117, 20186−20192

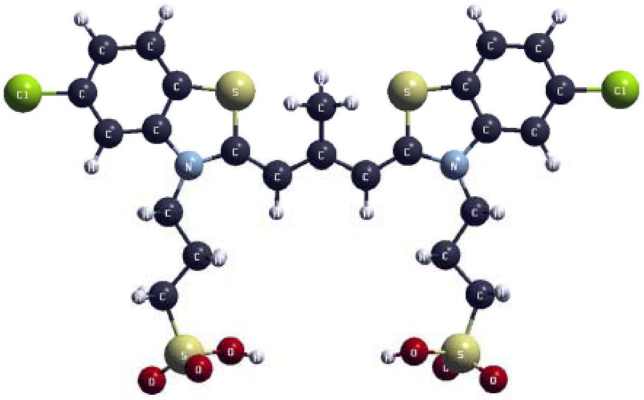

Figure 1. Schematic drawing of a single TCC molecule.

manipulating the aggregation morphology, for example, through adjustment of the dye concentration in solutions[3,5] by exploiting the counteraction size specificity in the electrolyte-induced aggregation[6] or by varying pH values.[18] Here we explore optical properties of films of TCC aggregates by using spectroscopic ellipsometry that allows us to evaluate real and imaginary parts of their frequency ω-dependent complex dielectric functions $\varepsilon(\omega) = \varepsilon'(\omega) + i\varepsilon''(\omega)$ utilizing the precise knowledge of the polarization state of the incident and reflected radiation.[19] Our results agree well with the picture of uniaxial anisotropy corresponding to two distinct dielectric functions: $\varepsilon_{\parallel}(\omega)$ for the dielectric response in the directions parallel to the film and $\varepsilon_{\perp}(\omega)$ for the direction perpendicular to the film. By performing ellipsometry over a wide spectral range (0.6−4 eV), we demonstrate strongly anisotropic responses of our thin films. In particular, the resonance feature assigned to J-aggregates is found to be polarized parallel to the film. The anisotropy is further confirmed by means of polarized infrared spectroscopy accompanied by a density-functional-theory (DFT) analysis of infrared absorption bands.

We then utilize the anisotropic dielectric functions derived from the ellipsometric measurements in model calculations of energy transfer rates from donor fluorophores into thin films of J-aggregates. These calculations demonstrate intricate dependences on the film thickness and distance to the donor that result from the strong and anisotropic dielectric resonance in the acceptor film.[20] Understanding particulars of energy transfer in such systems may be useful for engineering hybrid nanostructures that employ exceptional optical properties of J-aggregates.

METHODS

TCC dyes were purchased from Ryan Scientific. Dye solution was prepared by dissolving 10 mg of TCC in 1500 μL of methanol. The films were deposited on two different types of substrate surfaces: on SiO_2/Si and on Au. Before the film deposition, the dye solution was mixed by a magnetic spin bar for 10 min and sonicated for 10 min. Spin-coating was performed on Laurell WS-400-6NPP spin-coater. A total of 150 μL of the freshly prepared dye solution was injected onto the center of the sample while it was spinning at a speed of 10000 rpm, with the rotation maintained for 1 min. SiO_2 surfaces were first cleaned in a piranha solution (H_2O_2/H_2SO_4 in a proportion of 1:3) at 80 for 30 min. For Au surfaces, we used substrates that consisted of a 500 nm Au layer deposited on Si surfaces. Au surfaces were subjected to UV-ozone cleaning for 30 min prior to the deposition of TCC.

Jobin-Yvon Horiba Uvisel spectroscopic ellipsometer was used for characterization of the samples in 0.6−4 eV spectral range (referred to as VIS-ellipsometry). To model the ellipsometric data obtained from TCC layers, an anisotropic layer-model was assumed.[14,19] As consistent with the data, we adopt here uniaxial anisotropy wherein there are only two different components in the diagonalized dielectric tensor: $\varepsilon_{\parallel}$ for the two directions parallel to the layer and $\varepsilon_{\perp}$ for the direction perpendicular to the layer. Note that we use this notation throughout this paper: with index $\parallel$ referring to the directions parallel to the layer and index $\perp$ to the perpendicular direction. The dielectric response of the layer is thus characterized by two dielectric functions: $\varepsilon_{\parallel}(\omega)$ and $\varepsilon_{\perp}(\omega)$. Each of them is modeled as a sum of contributions from Lorentz oscillators:[21,22]

$$\varepsilon(\omega) = \varepsilon_{\infty} + \sum_n \frac{f_n \omega_n^2}{\omega_n^2 - \omega^2 - i\gamma_n \omega} \quad (1)$$

In this representation, ε_{∞} is the background constant, while each of the oscillators is characterized by its resonance frequency ω_n and damping γ_n and strength f_n constants. These parameters are found from the fits to the experimental data for each of $\varepsilon_{\parallel}(\omega)$ and $\varepsilon_{\perp}(\omega)$ functions.

All ellipsometric data was obtained under a nitrogen atmosphere. To ensure that the photosensitive TCC molecules were not damaged after each ellipsometric scan, a subsequent ellipsometric data set was obtained in order to verify that the peak intensity and peak positions of the absorption bands are stable and reproducible. All data was obtained at three angles of incidence: 70, 74, and 78° for SiO_2/Si surfaces. The fitting routine involved a fit to the data for all three angles of incidence for TCC on silicon, which enabled a high-accuracy determination of the thickness and the parameters of the dielectric functions in eq 1. Next, TCC on the Au surface data was considered. The dielectric parameters of eq 1 were kept fixed to the values obtained for TCC on SiO_2/Si substrates, while the parameter for thickness was allowed to vary when the fit was performed for 3-angles of incidence data obtained from TCC/Au substrates. This way, the consistency between the different data sets was ensured. Indeed, the ellipsometric thickness of the films thus determined was found to be in the range of ≃4−4.5 nm on both substrates.

IR absorption spectra were recorded in the reflection mode using a Nicolet 6700 FTIR spectrometer from Thermo Scientific equipped with a MCT-B detector. Reference spectra were obtained using identical samples prior to the attachment of the TCC dyes. All IR data was obtained under nitrogen atmosphere.

Both optical and atomic force microscopy (AFM) were used for the studies of the film morphology. AFM was performed using the tapping mode of a Dimension 3100 microscope from Nanoscope. The actual dense TCC films used for ellipsometric characterization exhibited a high degree of homogeneity and resulting low height-contrast without clearly resolved structures. When the TCC solution was substantially diluted (10 times amount of methanol), the deposition, however, resulted in a different morphology with separable larger-scale fiber-like structures spread on the sample surface, whose images could be resolved.

dx.doi.org/10.1021/jp407056t | J. Phys. Chem. C 2013, 117, 20186−20192

DFT calculations. The calculations were performed using DFT within the generalized gradient approximation (GGA) as implemented in the Vienna ab initio simulation package[23] (VASP). The electron-ion interaction was described within the projector-augmented wave scheme.[24] The electronic wave functions were expanded into plane waves up to a kinetic energy of 400 eV. The supercell used here consisted of 63 atoms. The atoms were allowed to relax until the forces on the atoms are below 10 meV/Å. The Brillouin zone integration was performed using 4 × 4 × 4 mesh within the Monkhorst-Pack scheme. The PBE functional was used to describe the electron exchange and correlation energy within the GGA. Eigenmodes were calculated by the force-constant approach, diagonalizing the mass weighted second derivative Hessian matrix.

EXPERIMENTAL RESULTS AND DISCUSSION

Figure 2a,b exemplify the ellipsometric data obtained from the TCC films on Au and on SiO_2/Si surfaces, respectively. Shown

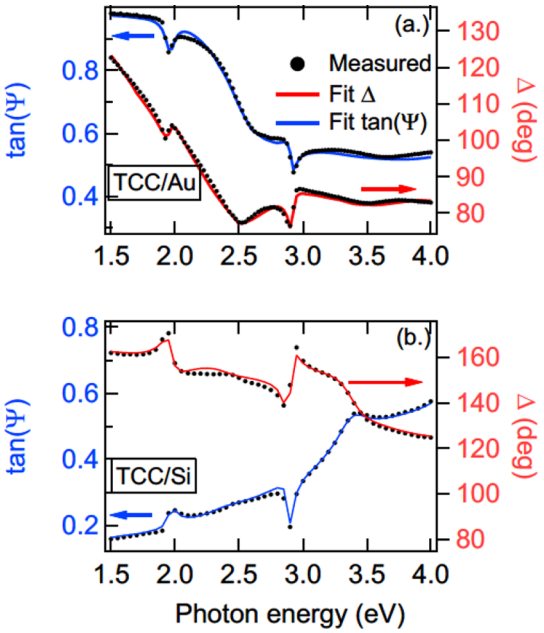

Figure 2. (a) Ellipsometric parameters tan Ψ (blue, left axis) and Δ (red, right axis) for TCC deposited on the Au surface. (b) Ellipsometric data for TCC on the SiO_2/Si surface. The data shown in this figure was obtained at 70 angle of incidence and display both experimental points and the model fit within the uniaxial anisotropic model. The fitted parameters included Lorenz oscillator parameters in eq 1 along with the film thickness as discussed in the text.

in this figure are standard[19,21] ellispometric parameters tan Ψ and Δ as functions of the photon energy $\hbar\omega$. It is noticed that the measured tan Ψ data exhibit peak-shapes characteristic of the response of thin films with uniaxial anisotropy when deposited on metallic and semiconducting surfaces.[12,25] Specifically, tan Ψ data obtained from TCC on Au surfaces exhibit two peak-down features while on SiO_2/Si, the response results in peak-up and peak-down features. This is typical for materials with anisotropic dielectric functions: the peak-up features in tan Ψ spectra from thin anisotropic films deposited on nonmetallic surfaces are due to the electronic transition dipole moments parallel to the surface and peak-down features are due to those perpendicular to the surface.

These considerations are confirmed by the quantitative analysis: the experimental data is well fitted within the framework of the uniaxial anisotropic model. The model fit, also shown in Figure 2, was achieved with two Lorentz oscillators in eq 1 for the dielectric function $\varepsilon_{\parallel}(\omega)$ parallel to the film surface and with one oscillator for the function $\varepsilon_{\perp}(\omega)$ in the perpendicular direction. These dielectric functions (utilizing parameters derived from the fit) are displayed in Figure 3 separately for their real $\varepsilon'(\omega)$ and imaginary $\varepsilon''(\omega)$

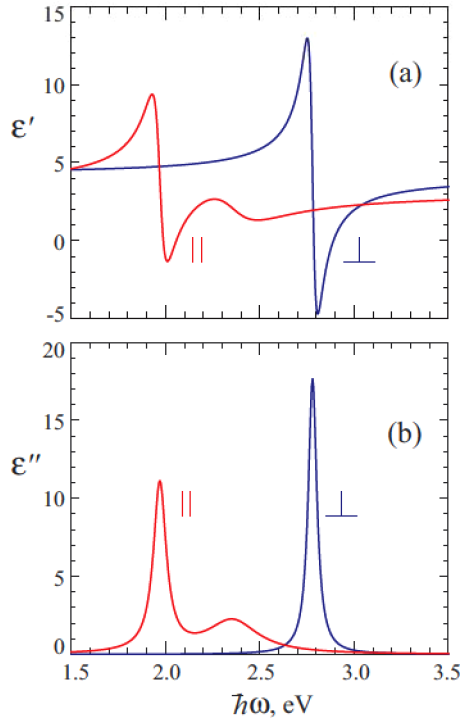

Figure 3. (a) Real and (b) imaginary parts of the frequency-dependent components of the dielectric tensor as derived from the ellipsometric measurements. Red lines (symbol ||) refer to the directions parallel to the film ($\varepsilon_{\parallel}$), and blue lines (symbol ⊥) to the direction perpendicular to the film ($\varepsilon_{\perp}$).

parts. The strongly anisotropic character of the dielectric response is evident in this figure as well as strong absorption resonances. As an example of numerical values, the fitted parameters for the lower energy oscillator in $\varepsilon_{\parallel}(\omega)$ include ε_{∞} = 3.05, the oscillator resonance energy $\hbar\omega_1$ = 1.97 eV, damping $\hbar\gamma_1$ = 0.082 eV, and strength f_1 = 0.45.

We have also attempted the effective medium approach (EMA) modeling of the obtained experimental ellipsometric data with a variable amount of air-inclusion voids considered as another optimization best-fit parameter. The corresponding model analysis would then show a convergence to the no-voids material representation of the film. The homogeneous (anisotropic) layer model thus resulting is consistent with the homogeneous pictures of the dense films observed in microscopic measurements.

The existence of strong resonances polarized in parallel and perpendicular directions and their energy positioning are indicative of the mixed nature of the deposited TCC films that contain both J- and H-aggregates (Figure 4). Indeed, the resonance energies of ≃1.97 eV (629 nm) and ≃2.78 eV (446 nm) are consistent with the J- and H-aggregate assignments made by Yao et al.[6] According to ref 6, TCC monomers in

dx.doi.org/10.1021/jp407056t | J. Phys. Chem. C 2013, 117, 20186−20192

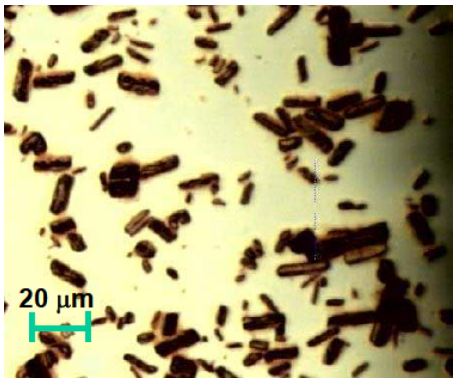

Figure 4. Optical microscope picture of the larger-scale fiber-like structures, as deposited on SiO_2/Si, from a dilute solution of TCC aggregates.

solutions exhibit an absorption band at 548 nm, while the absorption peak of J-aggregates is observed at 636 nm and the absorption band of H-aggregates is expected to be at 477−488 nm. A weaker absorption feature observed in our films (Figure 3b) at energy ≃2.36 eV (525 nm), thus, likely corresponds to nonaggregated or partially aggregated TCC molecules. One of the most important parameters to gain the control over the J- and H-type of aggregation in solutions is the solution concentration.[3,5] However, once the solution is subjected to spin-coating to form thin films on the surfaces, this notion cannot be directly applied due to the absence of the liquid solvent in thin films. While our solution concentration was tuned to contain J-aggregates, upon the spin-coating, a mixed nature of aggregates in the deposited thin films became apparent, where the varying angle of slippage between successive molecular planes could dictate the appearance of J- or H-aggregates.

It is natural to expect that, in the film deposition process, molecular aggregate columns would preferentially be oriented along the film surface. Yao et al.[5] discussed the molecular arrangement corresponding to a fiber-like morphology. We have not been able to resolve such structures in our dense homogeneous thin films. Larger-scale fiber-like structures have been, however, observed when deposited from very diluted solutions, as exemplified in Figure 4. Apparently the agglomeration may also depend on the concentration. A systematic study of the evolution of the aggregation and the morphology of thin films upon deposition from solutions of varied concentrations would be a useful research topic. The dense films do not show any large-scale orientational anisotropy in the film plane. This is consistent with the assumption of the isotropic distribution of orientations of aggregate filaments in the plane and, thus, with the uniaxial optical anisotropy of such films. In earlier studies of molecular aggregates,[17,18] it was proposed that J-aggregates are expected to exhibit the transition dipole moment parallel to the filaments while in H-aggregates, the electronic transition dipole moment would be perpendicular to the filament axis. Our anisotropic resonance data in Figure 3 is consistent with these expectations if the low-energy resonance is assigned to J-aggregates and the high-energy one to H-aggregates correspondingly oriented with respect to the film plane. Apparently, nonaggregated molecules also experience preferential orientation of their planes along the film leading to a smaller peak in $\varepsilon_{\parallel}(\omega)$ at intermediate energies.

The anisotropic response is also observed in the polarized IR spectroscopy. Figure 5 shows polarized IR absorption spectra

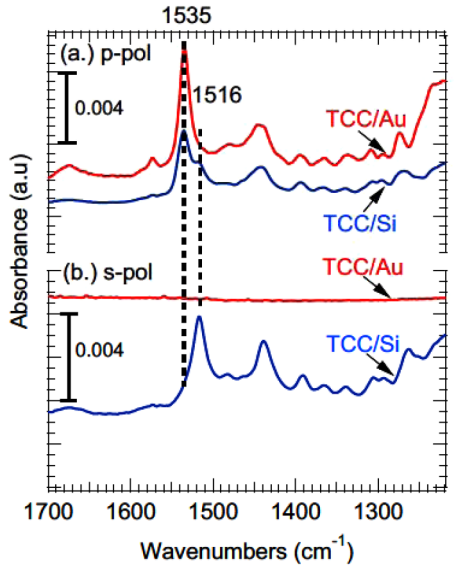

Figure 5. IR absorption data derived from TCC deposited on gold (red) and SiO_2/Si (blue) with (a) *p*-polarized and (b) *s*-polarized IR light. Polarization sensitive absorption bands at 1535 and 1516 cm^{-1} are marked. The data was obtained in the reflection mode at 82 angle of incidence.

derived from TCC deposited on Au and on SiO_2/Si surfaces with the *p*- and *s*-polarized incoming IR radiation. Theoretical results for the frequencies of the vibrational modes, as calculated by DFT, are listed in Table 1. The *p*-polarized IR spectra are characterized by two prominent absorption bands: at 1535 cm^{-1} (tentatively assigned to the calculated in-plane

Table 1. Infrared Frequencies Based on the DFT Analysis of a Monomer TCC Molecule

calcd frequency (cm^{-1})	assignment
1571	ring stretch, sym
1541	ring stretch, sym
1489	CH_2 deformation
1476	CH_2 deformation
1464	CH_3 deformation
1454	ring stretch, sym
1434	C═C stretch, C−N−C stretch, all in plane
1420	CH_2 deformation
1403	ring stretch, asym
1391	ring stretch, asym; C−C stretch; C−N stretch
1376	CH_3 umbrella mode
1348	ring stretch, sym
1335	CH_2 rock
1328	S═O stretch, asym
1319	S═O stretch, asym; CH−C stretch, sym; CH_2 deformation
1298	CH−C stretch, sym
1277	CH_2 wagging
1272	N−CH_2 stretch
1254	CH_2 rocking
1247	N−CH_2 stretch
1232	CH_2 deformation

dx.doi.org/10.1021/jp407056t | J. Phys. Chem. C 2013, 117, 20186−20192

vibrations at 1541 cm^{-1}) and at 1516 cm^{-1} (tentatively assigned to the theoretical out-of-plane vibrations at 1489 cm^{-1}). The spectrum obtained from the TCC/SiO_2/Si sample shows that the band at 1516 cm^{-1} is approximately half of the intensity of the strongest band at 1535 cm^{-1}. At the same time, the band at 1516 cm^{-1} is completely absent from the *p*-polarized spectrum derived from the TCC/Au sample. It is evident from Figure 5 that this cannot be related to lower SNR as the other peaks appear at comparable intensities. Moreover, the band at 1535 cm^{-1} is absent from the data obtained from the TCC/SiO_2/Si sample when *s*-polarization is used (on the metallic Au surface, no absorption bands were observed with the *s*-polarization in accordance with the surface selection rule). These observations then indicate that the band at 1516 cm^{-1} must possess a transition dipole moment parallel to the film surface, while the band at 1535 cm^{-1} is perpendicular to it. Based on the DFT analysis of a *monomer* TCC molecule, these absorption bands have been tentatively assigned to, respectively, in-plane and out-of-plane vibrational modes. The observation of the in-plane molecular vibrations perpendicular to the film and of the out-of-plane molecular vibrations parallel to the film would thus suggest their origination from the H-type aggregates of TCC molecules: with the stack of molecules whose planes are perpendicular to the columnar axis that is parallel to the film surface. More involved calculations of vibrational spectra in J- and H-aggregated structures may be needed to further clarify the role of intermolecular interactions on the positioning and polarization of their IR bands.

APPLICATIONS TO ENERGY TRANSFER

The strong absorption in J-aggregates makes them attractive objects for applications in the capacity of energy acceptors in energy-transfer-based hybrid structures[8] and, in fact, very efficient energy transfer (ET) was reported[10] from nanocrystal quantum dots to J-aggregates. Nonradiative (Förster-like[26−28]) energy transfer (NRET) into thin films of J-aggregates may have interesting features arising due to the strong interaction between individual acceptor species,[20] as we will illustrate here with theoretical calculations utilizing the data of Figure 3 derived from our measurements. Our example involves energy transfer from a point-like electric-dipole emitter (energy donor representing, for example, a quantum dot or a molecular fluorophore) in the vicinity of an absorbing (energy acceptor) layer shown schematically in Figure 6.

Experimentally, energy transfer is frequently assessed via measurements of the spontaneous decay rate of the donor excitation.[28] When in vacuum, the lifetime τ_0 and decay rate $\Gamma_0 = 1/\tau_0$ of the emitter fluorescence is determined by radiative transitions[29] as

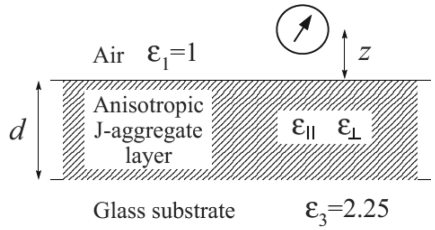

Figure 6. Schematics of the considered problem of energy transfer from a randomly oriented point-electric-dipole emitter into an anisotropic energy acceptor layer on the top of a glass substrate.

$$\Gamma_0 = k_0^3|\mathbf{p}|^2/3\pi\varepsilon_0\hbar$$

where $k_0 = \omega/c$ is the emission wavenumber and $\mathbf{p}$ the (effective) dipole transition moment. In the vicinity of polarizable media, the electromagnetic decay rate of the donor excitation can be substantially modified. A powerful approach was developed to evaluate the decay rate, which is based on methods of classical electrodynamics, and many detailed results are available for stratified geometries, see, for example, reviews in ref 29 and, particularly for anisotropic media, ref 30. We apply this approach to our layered geometry of Figure 6. For the donor dipole positioned at distance z from the top surface, the semiclassical analysis shows that the electromagnetic decay rate is modified to Γ, such that

$$\frac{\Gamma}{\Gamma_0} = 1 + \mathrm{Re}\int_0^\infty \frac{sds}{2\sqrt{1-s^2}}[(2s^2-1)r^{(p)}(s) + r^{(s)}(s)] \exp(2ik_0z\sqrt{1-s^2}) \quad (2)$$

The decay rate of a dipole generally depends on its orientation; eq 2 is a result of averaging eq (10.26) of ref 29 over random dipole orientations. Here $r^{(s)}$ and $r^{(p)}$ are the reflection coefficients for respectively *s*- and *p*-polarized waves that contain the information on the dielectric properties of the whole substrate structure. Specifically for our three-layer structure, these coefficients would be determined by reflective properties of two interfaces: r_{12} for the Air/J-aggregates and r_{23} for the J-aggregates/Glass boundaries:

$$r = \frac{r_{12} + r_{23}\exp(2ik_{2\perp}d)}{1 + r_{12}r_{23}\exp(2ik_{2\perp}d)} \quad (3)$$

where $k_{2\perp}$ is the component of the wave vector in the J-aggregate layer perpendicular to its plane (see eq (10.20) of ref 29). All these need to be determined for the respective polarized waves, taking into account anisotropy of this layer 2.

Upon reflection/refraction at the planar interface, the in-plane (parallel to the interface) components of the wave vector are conserved. The integration variable s in eq 2 relates magnitude $k_\parallel$ of those in-plane components to the vacuum wavenumber k_0 as $k_\parallel(s) = sk_0$. Correspondingly, in the isotropic parts of the structure (layers i = 1 and 3), the perpendicular components of the wave vector are found as

$$k_{i\perp}^2 = (\varepsilon_i - s^2)k_0^2 \quad (4)$$

they are, of course, the same for *s*- and *p*-polarized waves. We use dielectric constants $\varepsilon_1 = \varepsilon_{1\parallel} = \varepsilon_{1\perp} = 1$ for the air and $\varepsilon_3 = \varepsilon_{3\parallel} = \varepsilon_{3\perp} = 1.5^2$ for the glass substrate. In the anisotropic (assumed uniaxial) layer of J-aggregates, however, where dielectric functions $\varepsilon_{2\parallel} = \varepsilon_\parallel$ and $\varepsilon_{2\perp} = \varepsilon_\perp$, *p*- and *s*-polarized waves would have different perpendicular components:

$$k_{2\perp}^{(p)2} = \left(\varepsilon_\parallel - \frac{\varepsilon_\parallel}{\varepsilon_\perp}s^2\right)k_0^2 \quad (5)$$

and

$$k_{2\perp}^{(s)2} = (\varepsilon_\parallel - s^2)k_0^2 \quad (6)$$

It is convenient to write down reflection coefficients for each of the interfaces between layers i and j in the common uniaxial form, as appropriately modified from the respective isotropic expressions (formula 2.49 of ref 29):

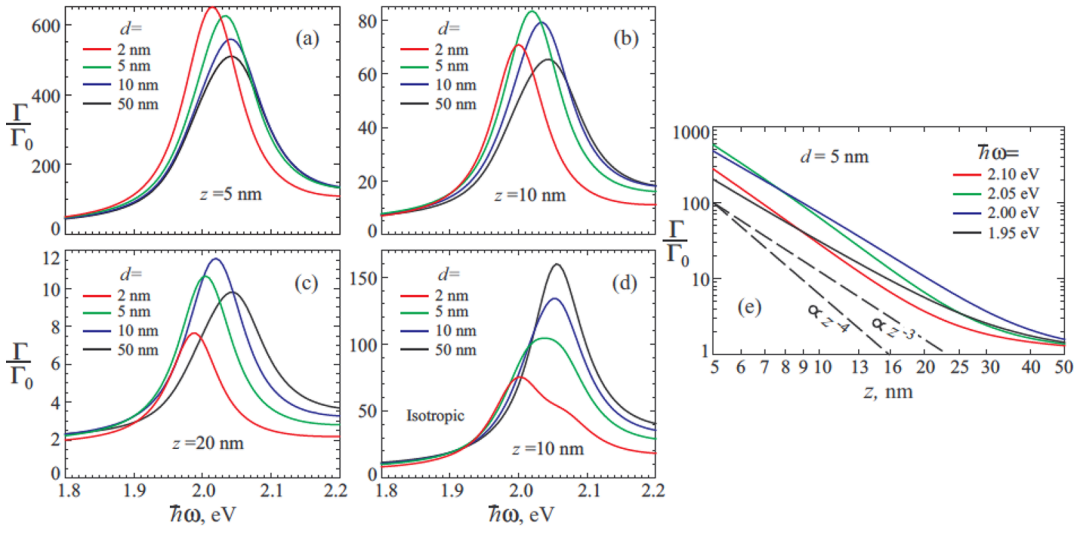

Figure 7. Acceleration of the spontaneous decay of the donor excitation with energy $\hbar\omega$ in the vicinity of the resonance of dielectric function $\varepsilon_{\parallel}(\omega)$ in Figure 3. (a–c) Acceleration of the decay as a function of the donor energy $\hbar\omega$ for anisotropic layers of different (indicated) thicknesses d and fixed distances z of (a) 5, (b) 10, and (c) 20 nm from the donor to the layer. (d) What the acceleration of the decay would be if the layer had an isotropic resonance with $\varepsilon_{\perp} = \varepsilon_{\parallel}$ and is to be compared with (b). (e) Double-logarithmic plot showing the relative decay rates as a function of the distance z from the anisotropic layer of d = 5 nm for few (indicated) donor energies. The dashed lines are guides to the eye for the slopes corresponding to z^{-4} and z^{-3} distance scaling.

$$r_{ij}^{(p)} = \frac{k_{i\perp}^{(p)}\varepsilon_{j\parallel} - k_{j\perp}^{(p)}\varepsilon_{i\parallel}}{k_{i\perp}^{(p)}\varepsilon_{j\parallel} + k_{j\perp}^{(p)}\varepsilon_{i\parallel}} \tag{7}$$

and

$$r_{ij}^{(s)} = \frac{k_{i\perp}^{(s)} - k_{j\perp}^{(s)}}{k_{i\perp}^{(s)} + k_{j\perp}^{(s)}} \tag{8}$$

Using eqs 5 and 7 in eq 3 would then yield the structure reflection coefficient $r^{(p)}$; for coefficient $r^{(s)}$, eqs 6 and 8 are employed.

The illustrative data displayed in Figure 7 have been computed by applying the above formalism for specific geometric parameters and utilizing dielectric functions $\varepsilon_{\parallel}(\omega)$ and $\varepsilon_{\perp}(\omega)$ from Figure 2 in the spectral vicinity of the J-aggregate resonance that is polarized parallel to the film. The computations have been performed via a direct integration in eq 2, over all possible "incidence angles". Figure 7a–c display the results of calculating eq 2 as a function of the donor excitation energy $\hbar\omega$ for various thicknesses d of the J-aggregate layer and distances z from the donor to the layer. It is clear from these panels that the donor excitation decay rate is dramatically affected by energy transfer into J-aggregate films, and details of ET rates, as a function of system parameters, can be quite intricate. One interesting and somewhat counter-intuitive feature is that over a range of frequencies ω, ET into thinner layers can be more efficient than ET into thicker layers, this is, for example, particularly striking in Figure 7a, where in the region of $\hbar\omega \lesssim 2.2$ eV the decay into a 2 nm thick layer is the fastest example. We have recently shown[20] that this type of counterintuitive behavior is characteristic of NRET into acceptor layers with large $|\varepsilon(\omega)|$ (e.g., close to resonances) and it gets more accentuated in the presence of the intrinsic layer anisotropy taking place here. To illustrate the role of the dielectric anisotropy, Figure 7d shows the results of calculations for the same distance z as in Figure 7b, but for an isotropic resonance, that is, with $\varepsilon_{\perp}(\omega)$ taken equal to $\varepsilon_{\parallel}(\omega)$. The difference between results in Figure 7d and b is evident both in numerical magnitudes and in the exhibited layer thickness dependence. The calculations suggest that some kind of NRET engineering might be possible for such systems where geometrical parameters are better adjusted to the spectral properties of the donor and acceptor. The proper assessment of optical anisotropy of the acceptor layer is evidently important for such engineering. Figure 7e further illustrates intricacies of ET in the vicinity of a strong dielectric resonance of the acceptor layer by displaying a transition-frequency dependent scaling with distance z. The results of calculations are to be compared with scalings $\propto z^{-4}$ and $\propto z^{-3}$ ordinarily discussed[31] in connection with NRET into, respectively, thin ($d \ll z$) and thick ($d \gg z$) acceptor layers. We note here that for broad donor emission lines, decay rates need to be averaged over the donor emission spectrum, which may result in washing out some of the discussed features.

SUMMARY

We used spectroscopic ellipsometry and polarized IR spectroscopy to explore optical properties of thin films of aggregated TCC dyes deposited on different surfaces. The experimental results reveal a strongly anisotropic behavior of the films that was quantified by means of two dielectric functions: $\varepsilon_{\parallel}(\omega)$ for the directions parallel to the film and $\varepsilon_{\perp}(\omega)$ for the direction perpendicular to it, over a wide range of frequencies. The studied TCC films exhibit both J-aggregate and H-aggregate absorption bands with different polarization properties. A strong dielectric resonance arising from the J-aggregate electronic excitations was found to be polarized along the film. This is consistent with the picture of the molecular aggregates being preferentially oriented parallel to the film surface.

We also employed the measured anisotropic dielectric functions in model calculations of energy transfer (ET) from small donor fluorophores into thin layers of J-aggregate acceptors. The model results illustrate interesting effects of a strong anisotropic dielectric resonance on ET in its dependence

dx.doi.org/10.1021/jp407056t | J. Phys. Chem. C 2013, 117, 20186–20192

on the layer thickness and distance from the layer. Accurate determination of the anisotropic optical constants can thus become important to engineer ET-based hybrid optoelectronic nanostructures utilizing exceptionally strong oscillator strengths and narrow fluorescence profiles of the dye aggregates for light-emitting and photon harvesting applications.

AUTHOR INFORMATION

Corresponding Author

*E-mail: katynko@gmail.com; anton.malko@utdallas.edu.

Notes

The authors declare no competing financial interest.

REFERENCES

(1) Kobayashi, T. *J-Aggregates*; World Scientific: Singapore, 1996.

(2) Harrison, W. J.; Mateer, D. L.; Tiddy, G. J. T. Liquid-Crystalline J-Aggregates Formed by Aqueous Ionic Cyanine Dyes. *J. Phys. Chem.* **1996**, *100*, 2310−2321.

(3) Behera, G. B.; Behera, P. K.; Mishra, B. K. J. Cyanine Dyes: Self Aggregation and Behaviour in Surfactants. *J. Surf. Sci. Technol.* **2007**, *23*, 1−31.

(4) Mishra, A.; Behera, R. K.; Behera, P.; Mishra, B. K.; Mehera, G. B. Cyanines During the 1990s: A Review. *Chem. Rev.* **2000**, *100*, 1973.

(5) Yao, H. S.; Kagoshima, Y.; Kitamura, S.; Isohashi, T.; Ozawa, Y.; Kimura, K. Superstructures of Mesoscopic Monomolecular Sheets of Thiacyanine J-Aggregates in Solution. *Langmuir* **2003**, *19*, 8882−8887.

(6) Yao, H.; Isohashi, T.; Kimura, K. J. Electrolyte-Induced Mesoscopic Aggregation of Thiacarbocyanine Dye in Aqueous Solution: Counterion Size Specificity. *J. Phys. Chem. B* **2007**, *111*, 7176−7183.

(7) Bradley, M. S.; Tischler, J. R.; Bulovic, V. Layer-by-Layer J-Aggregate Thin Films with a Peak Absorption Constant of 10^6 cm^{-1}. *Adv. Mater.* **2005**, *17*, 1881−1886.

(8) Agranovich, V. M.; Gartstein, Y. N.; Litinskaya, M. Hybrid Resonant Organic−Inorganic Nanostructures for Optoelectronic Applications. *Chem. Rev.* **2011**, *111*, 5179−5214.

(9) Coe, S.; Woo, W.-K.; Bawendi, M. G.; Bulović, V. Electroluminescence from Single Monolayers of Nanocrystals in Molecular Organic Devices. *Nature* **2002**, *420*, 800−803.

(10) Zhang, Q.; Atay, T.; Tischler, J. R.; Bradley, M. S.; Bulović, V.; Nurmikko, A. V. Highly Efficient Resonant Coupling of Optical Excitations in Hybrid Organic/Inorganic Semiconductor Nanostructures. *Nat. Nanotechnol.* **2007**, *2*, 555−559.

(11) Walker, B. J.; Bulović, V.; Bawendi, M. G. Quantum Dot/J-Aggregate Blended Films for Light Harvesting and Energy Transfer. *Nano Lett.* **2010**, *10*, 3995−3999.

(12) Roodenko, K.; Rappich, J.; Yang, F.; Zhang, X.; Esser, N.; Hinrichs, K. Anisotropy in Hydrogen-Passivated and Organically Modified Nanoporous Silicon Surfaces Studied by Polarization Dependent IR Spectroscopy. *Langmuir* **2009**, *25*, 1445−1452.

(13) Hinrichs, K.; Gensch, M.; Esser, N. Analysis of Organic Films and Interfacial Layers by Infrared Spectroscopic Ellipsometry. *Appl. Spectrosc.* **2005**, *59*, 272A−282A.

(14) Hinrichs, K.; Silaghi, S. D.; Cobet, C.; Esser, N.; Zahn, D. R. T. Ellipsometry from Infrared to Vacuum Ultraviolet: Structural Properties of Thin Anisotropic Guanine Films on Silicon. *Phys. Status Solidi B* **2005**, *242*, 2681−2687.

(15) Gordan, O. D.; Friedrich, M.; Zahn, D. R. T. The Anisotropic Dielectric Function for Copper Phtalocyanine Thin Films. *Org. Electron.* **2004**, *5*, 291−297.

(16) Kawka, S.; La Rocca, G. C. Role of Anisotropy in The Förster Energy Transfer From a Semiconductor Quantum Well to an Organic Crystalline Overlayer. *Phys. Rev. B* **2012**, *85*, 115305/1−6.

(17) Kano, H.; Saito, T.; Kobayashi, T. Dynamic Intensity Borrowing in Porphyrin J-Aggregates Revealed by Sub-5-fs Spectroscopy. *J. Phys. Chem. B* **2001**, *105*, 413−419.

(18) Ohno, O.; Kaizu, Y.; Kobayashi, H. J-Aggregate Formation of a Water-Soluble Porphyrin in Acidic Aqueous Media. *J. Chem. Phys.* **2005**, *99*, 4128−4139.

(19) Azzam, R. M. A.; Bashara, N. M. *Ellipsometry and Polarized Light*; North-Holland Pub. Co: Amsterdam, 1977.

(20) Gordon, J. M.; Gartstein, Y. N. Dielectric Polarization, Anisotropy and Nonradiative Energy Transfer into Nanometer-Scale Thin Semiconducting Films. *J. Phys.: Condens. Matter* **2013**, in press.

(21) Tompkins, H. G.; Irene, E. A. *Handbook of Ellipsometry*; Springer: Heidelberg, 2005.

(22) Tolstoy, V. P.; Chernyshova, I. V.; Skryshevsky, V. A. *Handbook of Infrared Spectroscopy of Ultrathin Films*; Wiley-VCH: NJ, 2003.

(23) Kresse, G.; Furthmuller, J. Efficiency of Ab-Initio Total Energy Calculations for Metals and Semiconductors Using a Plane-Wave Basis Set. *Comput. Mater. Sci.* **1996**, *6*, 15−50.

(24) Kresse, G.; Joubert, D. From Ultrasoft Pseudopotentials to the Projector Augmented-Wave Method. *Phys. Rev. B* **1999**, *59*, 1758−1775.

(25) Gensch, M.; Roodenko, K.; Hinrichs, K.; Hunger, R.; Guell, A. G.; Merson, A.; Schade, U.; Shapira, Y.; Dittrich, T.; Rappich, J.; Esser, N. Molecule−Solid Interfaces Studied with Infrared Ellipsometry: Ultrathin Nitrobenzene Films. *J. Vac. Sci. Technol. B* **2005**, *23*, 1838−1842.

(26) Kuhn, H. Classical Aspects of Energy Transfer in Molecular Systems. *J. Chem. Phys.* **1970**, *53*, 101−108.

(27) Kuhn, H.; Försterling, H.; Waldeck, D. H. *Principles of Physical Chemistry*; Wiley: Hoboken, NJ, 2009.

(28) Lakowicz, J. R. *Principles of Fluorescence Spectroscopy*; Springer: Berlin, 2006.

(29) Novotny, L.; Hecht, B. *Principles of Nano-Optics*; Cambridge University Press: Cambridge, 2006.

(30) Chance, R. R.; Prock, A.; Silbey, R. In *Advances in Chemical Physics*; Rice, S. A., Prigogine, I., Eds.; Wiley: New York, 1978; Vol. *37*, pp 1−65.

(31) Barnes, W. L. Fluorescence Near Interfaces: The Role of Photonic Mode Density. *J. Mod. Opt.* **1998**, *45*, 661−699.